Supplementary material

Hearing restoration by a low-weight power-efficient multichannel optogenetic cochlear implant system

DOI: 10.1088/1741-2552/adf00f

Lukasz Jablonski[1,2,3,4,5,*,#], Tamas Harczos[1,2,*], Bettina Wolf[1,2,3], Gerhard Hoch[1,3],Lakshay Khurana[1,2,3,5,6], Alexander Dieter[1,3,7], Lennart Roos[1,3,8,9], Roland Hessler[10], Suleman Ayub[11], Patrick Ruther[11,12,13], and Tobias Moser[1,2,3,4,8,13,14,#]

[1] University Medical Center Göttingen, Institute for Auditory Neuroscience, Göttingen, Germany
[2] Auditory Neuroscience and Optogenetics Laboratory, German Primate Center, Göttingen, Germany
[3] University Medical Center Göttingen, InnerEarLab, Göttingen, Germany
[4] University Medical Center Göttingen, Else Kröner Fresenius Center for Optogenetic Therapies, Göttingen, Germany
[5] Junior Research Group “Computational Neuroscience and Neuroengineering”, Göttingen, Germany
[6] University of Göttingen, The doctoral program “Sensory and Motor Neuroscience”, Göttingen Graduate Center for Neurosciences, Biophysics, and Molecular Biosciences (GGNB), Göttingen, Germany
[7] University of Göttingen, Göttingen Graduate School for Neurosciences and Molecular Biosciences, Göttingen, Germany
[8] University of Göttingen, Cluster of Excellence “Multiscale Bioimaging: from Molecular Machines to Networks of Excitable Cells” (MBExC), Göttingen, Germany
[9] University Medical Center Göttingen, Department of Otolaryngology, Göttingen, Germany
[10] MED-EL, Innsbruck, Austria
[11] Department of Microsystems Engineering (IMTEK), University of Freiburg, Freiburg, Germany
[12] BrainLinks-BrainTools, Cluster of Excellence, University of Freiburg, Freiburg, Germany
[13] University of Göttingen, Collaborative Research Center 1690 (CRC1690), Göttingen, Germany
[14] Auditory Neuroscience & Synaptic Nanophysiology Group, Max-Planck-Institute for Multidisciplinary Sciences, Göttingen, Germany
* equal contribution
# corresponding authors: lukasz.jablonski@wp.eu (L.J.), tmoser@gwdg.de (T.M.)

Choice of the digital signal controller

Prior to starting development of the sound processor, we critically reviewed state-of-the-art DSCs to see which would qualify for the envisioned tasks. The initial benchmarking of DSCs was performed in 2016 and the shortlist included PIC32MZ2048EFH and PIC32MX795F512L (Microchip), KW40Z (Freescale) based on ARM Cortex M0, SAM4L (Atmel) based on ARM Cortex M4, and nRF52832 (Nordic Semiconductor) based on the ARM Cortex M4. A comparison of their key properties is provided in Supplementary table 1.

We compared and benchmarked the shortlisted systems in various ways. Since the most demanding of the envisioned tasks was the real-time audio processing, we started by benchmarking spectral decomposition methods on all platforms. For that, we implemented spectral decomposition via fast Fourier transform (FFT) and infinite impulse response (IIR) based filter banks in several ways including those optimized for the specific microarchitecture (like the CMSIS DSP library for the ARM-based systems [1]). First, for all filter bank variants we determined the filtering duration of 1 second of audio sampled at 48 kilosamples per second into 10, 20, and 32 quasi-logarithmically spaced bands followed by an envelope extraction and quantisation in time. This calculation yields a matrix of spectrotemporal data, which can serve as a basis for an *n*-of-*m*-like coding strategy (see main text, “2.3. Sound coding strategy”).

	PIC32 MZ2048EFH (Microchip)	PIC32 MX795F512L (Microchip)	KW40Z (Freescale)	SAM4L (Atmel)	nRF52832 (NordicSemi-conductor)
RAM size	512 kB	128 kB	20 kB	32 kB	64 kB
Non-volatile memory size	2048 kB	512 kB	160 kB	256 kB	256 kB
Max. clock speed	200 MHz	80 MHz	48 MHz	48 MHz	64 MHz
Adjustable clock speed	yes	yes	yes	yes	no
Floating point unit	present	-	-	-	present
Operating voltage	2.2–3.6 V	2.3–3.6 V	0.9–4.2 V	1.68–3.6 V	1.7–3.6 V
Connectivity	6× UART 5× I^2C 6× SPI	6× UART 5× I^2C 4× SPI	1× UART 2× I^2C 2× SPI	3× UART 4× I^2C 1× SPI	1× UART 2× I^2C 3× SPI
Audio interface	1× I^2S	-	-	1× I^2S	1× I^2S 1× PDM
ADC	12 bit 18 Msps	10 bit 1 Msps	16 bit 500 ksps	12 bit 300 ksps	12 bit 200 ksps
DAC	-	-	12 bit 60 ksps	10 bit 500 ksps	-
Built-in 2.4 GHz radio	no	no	yes	no	yes
Smallest SMD package	9×9 mm	9×9 mm	5×5 mm	7×7 mm	6×6 mm

Supplementary table 1. Comparison of the digital signal controller (DSC) specifications. Parameters most instrumental for the DSCs to be used as sound processor and driver for oCI/eCI are presented. There are more than 25-fold differences in random access memory (RAM) and about 12-fold differences in non-volatile memory (NVM) sizes, with more memory meaning more flexibility. The difference in maximum clock speed is less pronounced, and the nR52832 is the only DSC lacking the option to adjust clock speed at all. The range of operating voltage is widest for the KW40Z, while the PIC32 DSCs score with the richest set of interfaces like universal asynchronous receiver-transmitter (UART), inter-integrated circuit (I^2C) bus, and serial peripheral interface (SPI). Three DSCs feature inter-IC sound (I^2S) and/or pulse-density modulation (PDM) audio-specific interfaces aiding their use in the sound processing. All DSCs feature a built-in analogue-to-digital converter (ADC; Msps: megasamples per second, ksps: kilosamples per second) required for electrophysiological recordings and battery level monitoring. Three of them lack a digital-to-analogue converter (DAC) needed to precisely adjust the amplitude of electrical stimulation then requiring an external DAC. The two of the five shortlisted DSCs including a radio transceiver happen to have the smallest surface-mounted device (SMD) footprint, which was another key factor for the design. Data obtained from the data sheets provided by the manufacturers.

After choosing the ideal implementation for each individual system—as judged by the shortest calculation times for FFT and IIR—we determined the required clock speeds just for real-time spectral decomposition as a function of the number of frequency channels. Finally, based on measurements of electrical current and information from the specifications (com-

bined with data extrapolation where the clock speed was not adjustable as required), we estimated the required power as shown in Supplementary figure 1. Since CI systems require real-time audio processing for a long period of time, we deem the power efficiency of spectral decomposition to be very important for which nRF52832 (Nordic Semiconductor) outperformed the other processors for more than 20 frequency channels (Supplementary figure 1).

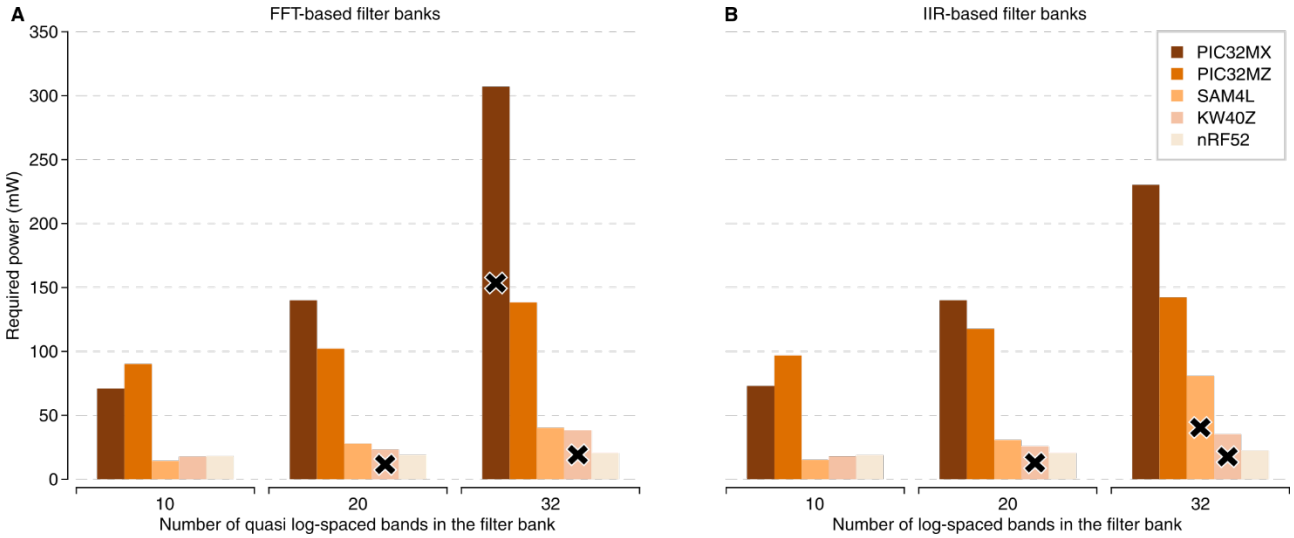

Supplementary figure 1. Comparison of power required just for real-time spectral decomposition by digital signal controllers (DSCs). (A) Required power for spectral decomposition via FFT-based filter bank operations. (B) Required power for spectral decomposition via IIR-based filter banks operations. Cross marks denote cases, where the required clock speed for real-time operation was higher than the specified maximum clock speed of the given system.

For the DSCs without built-in radio transceiver we considered various small commercial off-the-shelf Bluetooth Low Energy (BLE) modules to be connected via the Serial Peripheral Interface (SPI) and a few general purpose I/O (GPIO) pins for interrupt signalling. The extra space required by those modules belongs to the downsides of the radioless systems on a chip. First tests with the BLE protocol stack revealed that a sensible amount of working memory must be dedicated to the wireless functionality. Moreover, latencies can become relatively long when operating via BLE, which must be considered in the design of wireless control (see main text, section “2.4. Wireless control and communication protocol”).

In a final step, we tested the response speed and quality of the product support, reviewed the clarity and comprehensibility of documentation, as well as the availability of examples and public forums. Eventually, we selected the nRF52832 (Nordic Semiconductor) as implemented in the BL652 (Ezurio, formerly Laird Connectivity) module, which back then, in 2016, was the smallest form factor available on the market that implemented the full reference circuitry as specified by Nordic Semiconductor. While this system on a chip lacks a digital-to-analogue converter (DAC) and the possibility to adjust clock speed, it provides a range of useful

interfaces, an on-chip 2.4 GHz radio transceiver, and supports high computing power and efficiency. Last but not least, we found the documentation and support favourable.

Choice of the filter bank

Whenever the signal processor is in real-time sound encoding mode, it transfers audio samples from the PDM microphone to the RAM, spectrally decomposes the signal, and transforms it into patterns of activation of the oCI emitters or the eCI electrodes aiming to stimulate SGNs at the tonotopic positions that correspond to the frequencies contained in the sound signal. While sound capturing—once appropriately configured and started—operates by direct memory access and double buffering without substantial involvement of the CPU, the further processing of the audio samples places major demands on the computational power. For this reason, we carefully evaluated spectral decomposition via FFT- vs. IIR-based filter bank operations (Supplementary figure 1).

Because the optical or electrical stimulation channels are placed equidistantly on the cochlear implant, the employed filter bank should ideally have a quasi-logarithmic frequency resolution for the stimulation to match the tonotopic organisation of the cochlea. This is easily set up when using an IIR-based filter bank: with IIR filters the required computational power scales almost linearly with the number of required frequency channels. When using FFT, the increase of computational power as a function of frequency channels is less obvious: the real FFT implementation of the DSP library is very efficient, but it implies various overheads in our case. First of all, every block of input data needs to be multiplied by the values of a window function. Then, real-valued magnitudes need to be calculated from the complex spectral values, requiring not only multiplications and additions, but also the computationally more expensive square root calculation. Next, the resulting magnitudes, corresponding to the linearly spaced real FFT frequency bins, need to be combined to form quasi log-spaced channel frequencies, which requires further multiplications and additions. Finally, processing encompasses 50 % overlapping of the temporal analysis windows to not miss transients, which, as a consequence, doubles the required calculations. For these reasons, we chose an IIR-based filter bank for spectral decomposition. More specifically, we used the single precision floating point implementation of a biquadratic second order IIR (biquad) band-pass filter as the basic building block of our filter bank with quality factor of 12. We also evaluated the fixed-point implementation but found only a trend toward better performance at the same current consumption, while trading in a reduced dynamic range and noise artefacts due to rounding errors.

Optical stimulation circuitry

The oCI driver circuity employs a 16-channel digitally adjustable current sink (TLC5923, Texas Instruments Inc.) and an 8-channel analogue switch (ADG1414, Analog Devices) each controlled by the DSC via dedicated SPIs (SPI0 and SPI1, respectively, see Figure 2). This design enables matrix addressing of the oCI arrays with up to 128 channels: the common anode of the respective LED block (up to maximum 8 blocks) is selectively activated by the analogue switch. The individual LED within a block is selected and its light intensity is adjusted by the current sink, setting of the current level of each LED within a block (up to maximum 16 LEDs per block). Independent of the topology of the LED array, the DSC needs ~15 µs for internal commands to set up the LED array with the requested light intensities. The output of the oCI driver is accessible on the female pin header (CLE-110-01-G-DV, Samtec) for interfacing oCI probes (see Stimulation probes design). For the future probes employing matrix addressing [2], pin header with more contacts can be soldered (CLE-114-01-G-DV, Samtec).

Electrical stimulation circuitry

The eCI driver circuity employs a dual 16-channel multiplexer (MAX14661, Maxim Integrated) and a 12-bit DAC (AD5683, Analog Devices) driving a current source (AD8643, Analog Devices) to supply the charge balanced biphasic stimuli via a channel-dedicated capacitor to the selected electrode. The multiplexer and DAC are controlled by the DSC via dedicated SPIs (SPI0 and SPI1, respectively, see Figure 2). By the design of the eCI, the output of the eCI driver is limited to 10 channels accessible on the female pin header (CLE-107-01-G-DV, Samtec) for interfacing eCI probes (see Stimulation probes design).

Size, weight, and power consumption

The complete oCI/eCI sound processor and driver circuitry is built in a form of a cylinder accommodated in a low-weight (~6.5 g) and robust plastic enclosure made of Polyether ether ketone (PEEK). The inside diameter of the enclosure is 25 mm and its height 30 mm. The enclosure consists of a threaded head-mounted base (~1.5 g, Figure 1 C and D) fixed by dental acrylic and metal anchors to the skull of the animal, as well as a screwable cap (~5 g, Figure 1 B). This design allows for convenient installation of the device on the animal's head and battery replacement. The oCI/eCI sound processor and driver circuitry consists of two round multilayer rigid PCBs (Figure 1 B, E, and G), each 20 mm in diameter, carrying com-

mercial off-the-shelf electronic components on both sides, which were interconnected via PCB surface-mounted pin headers (top PCB: FTE-106-03-G-DV, Samtec; bottom PCB: CLE-106-01-G-DV, Samtec). The bottom PCB (closer to the animal's head) consists of the sound processor and oCI/eCI driver circuitry (Figure 2). It is connected to the head-mounted pin header to interface with the eCI or oCI. The top PCB consists of a battery bracket holding a lithium-ion battery (CP1654A3, VARTA Microbattery GmbH; for details see Selection of the battery), a step-down converter (TPS62240, Texas Instruments Inc.) for powering of the DSC, booster (MCP16251, Microchip Technology Inc.) for powering current source (in case of the eCI system) or LED driver (in case of the oCI system), and a circuit based on a nano-power comparator (MAX9117, Maxim Integrated) that shuts off powering when the battery voltage is too low to allow a reliable operation of the system. A flexible antenna for 2.4 GHz radio (FXP73, Taoglas) is wrapped around the PCBs assembly. The weight of both PCBs including battery and antenna is ~8 g and complete oCI/eCI system is ~15 g. The performance of the oCI/eCI system operating under battery powering is shown in Supplementary figure 2.

Selection of the battery

Seeking the low weight battery enabling reliable operation of the oCI/eCI systems, we tried various batteries starting with lithium coin cell CR1631, including hearing aid dedicated Zinc Air MERCURY-FREE (size p13 and p675, power one VARTA Microbattery GmbH), and cochlear implant dedicated series IMPLANT plus (size p675, power one VARTA Microbattery GmbH). Most of them failed for our purpose not being able to provide enough current for long term wireless operation in permanent receiving or transmitting mode where radio transceiver is always turned on (ShuttleBox paradigm with triggered predefined stimulation). Finally, we successfully employed a lithium-ion battery (CP1654A3, VARTA Microbattery GmbH). Battery testing running the ShuttleBox-like paradigm (see main text, section "Behavioural experiments paradigm") revealed 7–8 hours of the device operation. The discharge curve of the battery is shown in Supplementary figure 2 B.

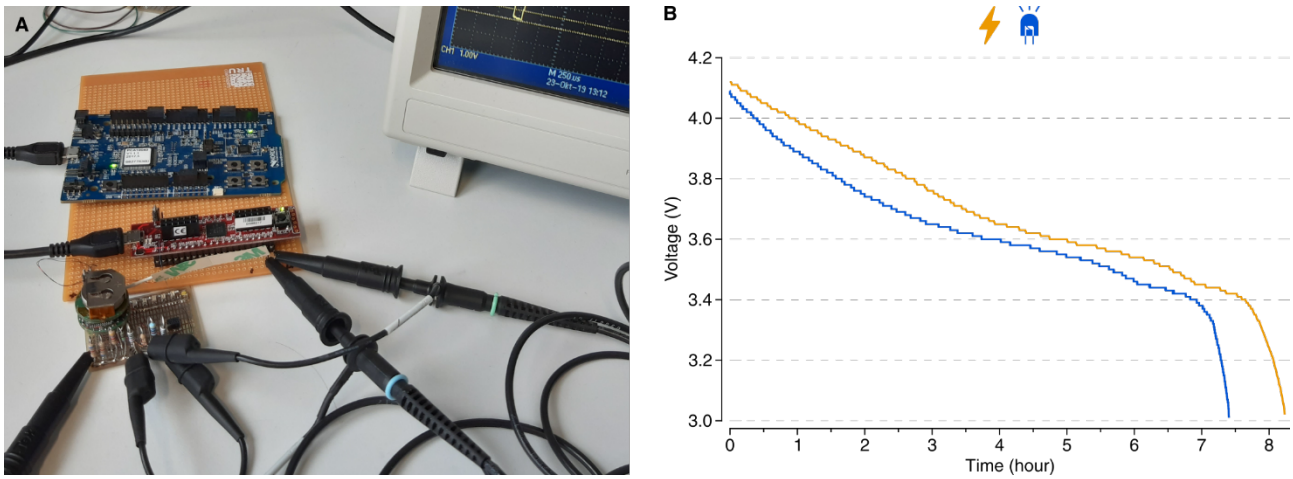

Supplementary figure 2. Test of the lithium-ion battery usage under operation in the eCI and oCI systems. (A) Photograph of the custom-build setup employing the most demanding paradigm of the ShuttleBox protocol and a 6.8 kΩ resistor in place of a single eCI channel simulating current injection into the cochlea or single LED of the oCI implant. (B) Corresponding discharge curves of the batteries of eCI (orange) and oCI (blue) systems showing continuous operation for 7–8 hours.

Testing was performed using MATLAB (MathWorks, Inc.) script simulating ShuttleBox experiment in which stimulation is triggered via ESB bridge for the maximum length of the response window and minimum inter-trial-interval of 10 s. This simulation is considered the most demanding scenario from the point of the view of power consumption in such ShuttleBox experiments. For eCI system, instead of implant and the animal, the 6.8 kΩ resistor, matching the average impedance of the electrode implanted into the animal, was used. For oCI system, oCI implant was used (see Stimulation probes design). Stimulus parameters were the same as in the experiments with animals for both systems except of number of channels stimulated simultaneously, here single channel for either eCI or oCI, as well as for eCI current intensity of 300 µA (~20 % of a maximum current possible for an eCI driver) and for oCI light intensity of 20 % of a maximum current possible for an oCI driver (~620 µA per LED). Current consumption of the device and voltage level of the battery were measured with custom-build setup consisting of Cmod CK1 (Digilent Inc.) and a current-shunt monitor INA186 (Texas Instruments Inc.) running custom-coded firmware sending data via UART interface to the PC (Supplementary figure 2 A).

Transfer characteristic of the sound processor's audio system

The audio quality of the sound processor is determined by the acoustic setup (e.g. positioning of the microphone, diameter of the acoustic vent in the PCB, acoustic shadow effects of the processor enclosure), the PDM microphone, and the processor's PDM interface.

To characterise the overall audio quality of the processor, we developed a program (stored as “Audio calibration mode” in the sound processor, see Figure 2) that analyses signals coming from the PDM microphone and forwards analysis results to a PC. For the analysis it uses a sampling rate of 50 ksps, a 512-point real-valued FFT with floating point precision based on the CMSIS DSP library [1], and Blackman-Harris window function.

In an acoustically shielded chamber (Industrial Acoustics) we used a single Tannoy Reveal 402 loudspeaker (± 3 dB linearity between 56 Hz and 48 kHz) driven by a Zoom UAC-8 audio interface (± 1 dB linearity between 20 Hz and 40 kHz at 96 ksps) to play back sound generated by a custom-coded MATLAB (MathWorks, Inc.) script. The distance between the centre of the loudspeaker and the sound processor was exactly 1 m. The sound pressure level was controlled for at the sound processor’s position with a calibrated Phonic PAA3 audio analyser.

Using script, we generated a sine sweep (chirp signal sweeping from 100 Hz to 30 kHz at 96 ksps sampling rate), which we played back at specific sound pressure levels (SPL) while the analysis program was running on the sound processor. The results for 95 dB SPL, 65 dB SPL, and silence (noise floor measurement) for frequencies between 200 Hz and 25 kHz are shown in Supplementary figure 3.

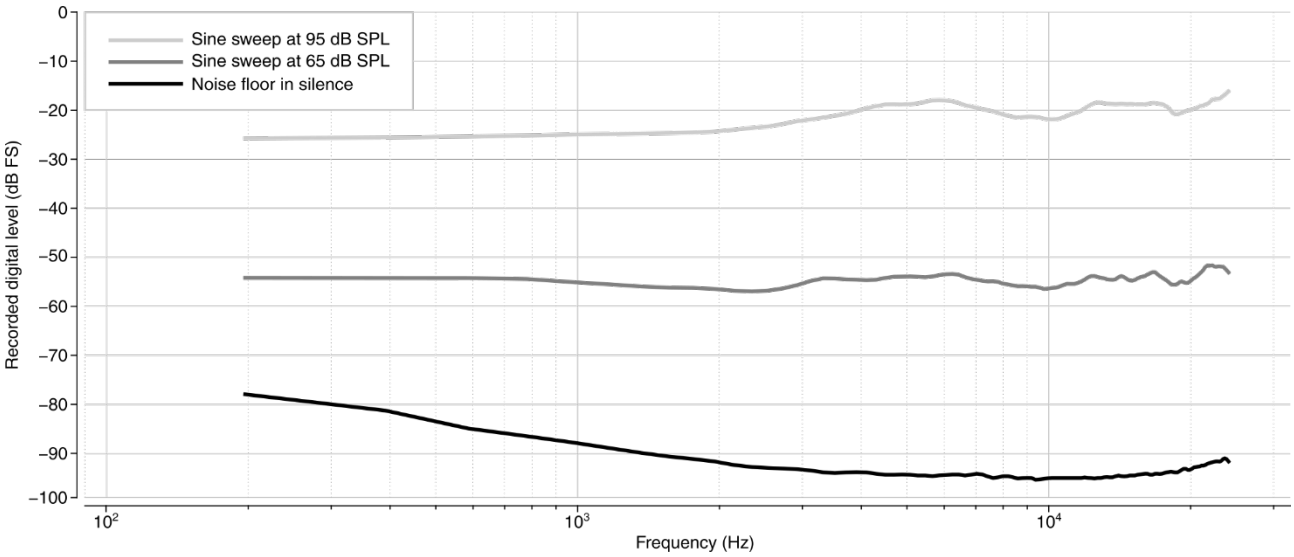

Supplementary figure 3. Transfer characteristics of the sound processor’s audio system at different sound pressure levels. Measurements of a noise floor in silence (black) and sine frequency sweep at: 65 dB SPL (light grey) and 95 dB SPL (dark grey).

Operating modes of MobileProcessor running NSV1 software

The NSV1 embedded software framework implements different operating modes realising requirements of different experiments (Supplementary table 2). Switching between operating modes is possible using a protocol based on Enhanced ShockBurst (ESB) or over a 2-wire port via universal asynchronous receiver-transmitter (UART).

MODE	CI type	Description
MODE1	oCI	Predefined optical stimulation upon trigger (Proof-of-concept)
MODE2	oCI	Predefined optical stimulation upon trigger
MODE3	-	Microphone calibration
MODE4	oCI	Real-time sound processing (CIS/*n*-of-*m*, up to 32 channels)
MODE5	-	CI fitting
MODE6	eCI	Predefined electrical stimulation upon trigger
MODE7	eCI	Real-time sound processing (CIS/*n*-of-*m*, up to 32 channels)
MODE8	oCI	Real-time sound processing (up to 32 channels)

Supplementary table 2. List of operating modes implemented in the NSV1 software framework running on the MobileProcessor. The NSV1 allows dynamic switching between operating modes using a protocol based on Enhanced ShockBurst (ESB) or over a 2-wire port via universal asynchronous receiver-transmitter (UART) using fixed-length commands in a form of a human-readable 15-character-long ASCII messages. Same communication commands are also used for any other settings and returning measurement (e.g.: impedance in eCI or LED open circuity detection in oCI) results.

Modes of operation of the MobileProcessor used in behavioural experiments with ShuttleBox in rats can be categorized into two main types (Supplementary figure 4). USB-to-ESB interface (yellow) to predefine parameters of the stimulation (number of pulses, pulse length, pulsing frequency, intensity, channel numbers) and trigger it for detection experiments (Figure 3, Figure 4, Supplementary figure 7), and audio interface (green) producing sound delivered to the PDM microphone of the MobileProcessor for experiments involving sound coding strategies (Figure 5, Supplementary figure 8).

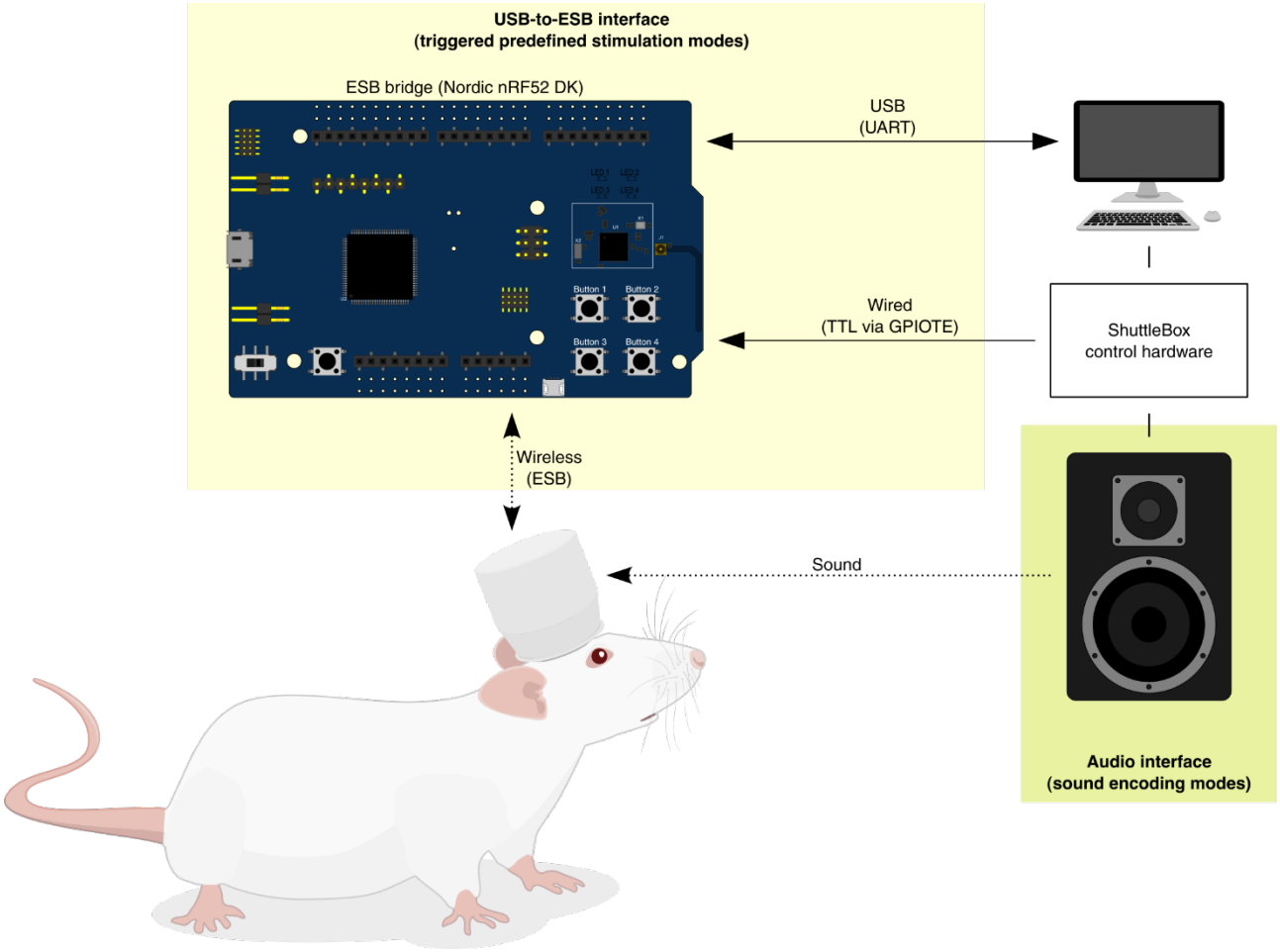

Supplementary figure 4. Illustration of two main operation mode types of the MobileProcessor used in behavioural experiments with ShuttleBox in rats. For detection experiments (Figure 3, Figure 4, Supplementary figure 7) USB-to-ESB interface (yellow) was used to predefine parameters of the stimulation (number of pulses, pulse length, pulsing frequency, intensity, channel numbers) and trigger it while for experiments involving sound coding strategies (Figure 5, Supplementary figure 8) audio interface (green) produced sound delivered to the PDM microphone of the MobileProcessor. Signal pathways are schematically represented by arrows; the orientation of the arrowheads indicate the signal direction. Solid lines indicate wired and dotted lines wireless connections.

Stimulation probes design

The eCI probes, based on previously described design [3], consisted of 2 linearly arranged intracochlear platinum sheet contacts and an extracochlear platinum-iridium reference ball electrode (Supplementary figure 5 A and B). All contacts were connected via lead wires to a 3-pin male connector (2 mm pitch) and are embedded into silicon. The intracochlear contacts were 0.3 mm in diameter each with a centre-to-centre pitch of 1 mm. To assure reproducibility of implantations across animals an array was marked with a black dot at a distance of 3 mm measured from the apical tip (Supplementary figure 5 B). The diameter of the silicone-encapsulated intracochlear and intrabullar part was 0.3 mm increasing to 0.9 mm at the extrabullar part to provide a stable submuscular connection. The silicone-encapsulated return electrode was 0.3 mm in diameter. These animal eCIs prepared by MED-EL, except the size and the number of stimulation sites, are virtually identical to implants used in human patients. Its 3-pin connector was interfaced with the head-mounted adaptor board to male pin header (FTE-107-03-G-DV, Samtec; (not present in Supplementary figure 5 A) that in turn was connected to the female pin header (CLE-107-01-G-DV, Samtec) of the driver circuitry.

The oCI probes, based on previously described design [4], consisted of 10 LEDs (C460TR2227-S2100, Cree), each 220 µm by 270 µm by 50 µm, spaced at a pitch of 350 or 450 µm along a polyimide carrier comprising wiring and LED contact pads encapsulated into silicone (Supplementary figure 5 C and D). Its ZIF connector (5020781362, Molex) was interfaced with the head-mounted adaptor board to male pin header (FTE-110-03-G-DV, Samtec; Supplementary figure 5 C) that in turn was connected to the female pin header (CLE-110-01-G-DV, Samtec) of the driver circuitry (as illustrated in Figure 1 C).

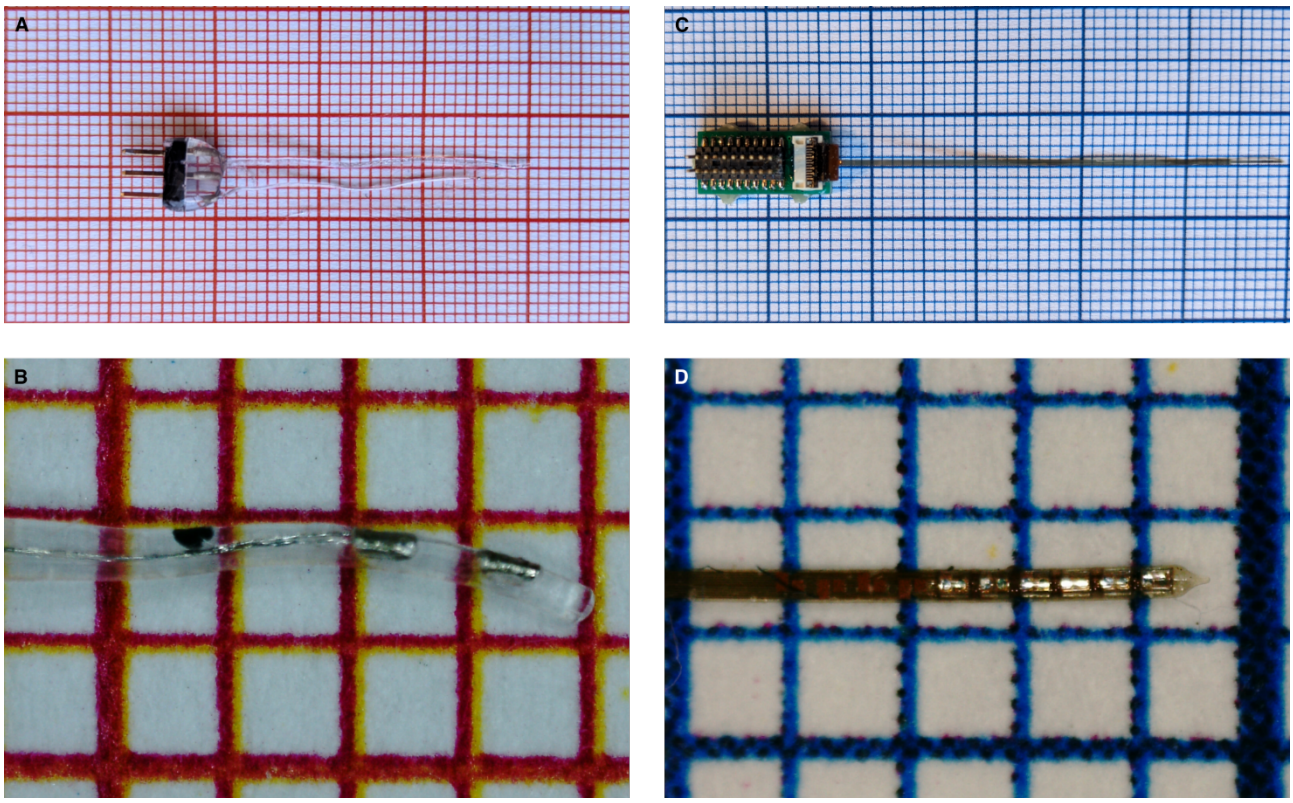

Supplementary figure 5. Design of the chronic eCI and oCI probes used in behavioural experiments. (A and B) Photographs of MED-EL's preclinical two-channel eCI [3]. (A) Two-channel eCI probe showing both intracochlear and return electrodes. (B) Close-up photograph of the intracochlear part with two electrode contacts and black insertion mark of the eCI. (C and D) Photographs of preclinical six-channel oCI. (C) Six-channel LED oCI connected to the adaptor board interfacing ZIF contact pads with the sound processor (left part). The design is identical to the ten-channel probes used in experiment except of lack of four basal LEDs. (D) Close-up photograph of the intracochlear part with six LEDs and contact pads for additional four LEDs (identical design was used in experiments except of all 10 LEDs were present as previously published [4,5]). Millimetre paper in the background.

AAV production

Recombinant viral vector purification was carried out as previously reported and its extensive description is available [6]. Briefly, triple transfection of HEK-293T cells was performed using the pHelper plasmid (TaKaRa, USA), trans-plasmid with the PHP.B capsid and cis-plasmid with CatCh [7] fused to enhanced yellow fluorescent protein (eYFP), under the control of human synapsin promotor. Cells were routinely screened for mycoplasma contamination. Viral particles were precipitated from culture supernatant with 40 % polyethylene glycol 8000 (Acros Organics, Germany) in 500 mM NaCl and combined with cell pellets for processing. Pellets were suspended in 500 mM NaCl, 40 mM Tris, 2.5 mM MgCl2, pH 8, and 100 Uml^{-1} of salt-activated nuclease (Arcticzymes, USA) at 37 °C for 90 minutes. Cleared lysates were purified using discontinuous iodixanol gradients (Optiprep, Axis Shield, Norway; 15%, 25%, 40%, and 60%) at 350,000 × g for 2.25 h. rAAV containing fractions were concentrated using Amicon filters (EMD, UFC910024) and formulated in sterile phosphate-buffered saline (PBS) supplemented with 0.001% Pluronic F-68 (Gibco, Germany). Viral vector titers were determined by the count of DNase I resistant vg using AAV titration kit (TaKaRa/Clontech) by qPCR (StepOne, Applied Biosystems) according to the manufacturer's instructions. Purity of produced viral vectors was assessed in silver stainings (Pierce, Germany) after gel electrophoresis (Novex 4–12% Tris-Glycine, Thermo Fisher Scientific) according to the manufacturer's instruction. Viral vector stocks were then stored at −80 °C until postnatally injected.

Postnatal AAV-injection into the rat cochlea

The injections of AAVs (see AAV production) were only conducted into the left cochlea of wistar wild-type rats via the round window at postnatal day 5 to 7. Here, rat pups were randomly selected for virus injections. All animals were frequently monitored throughout the injection procedure in regards of general isoflurane/air anaesthesia (3.5–5% for anaesthesia induction, 0.6–2% for maintenance), the absence of the hind-limb withdrawal reflex, the breathing rate as well as maintenance of physiological body temperature. Further, eye creme was applied and adjustments were made accordingly. Analgesia was provided by subcutaneous buprenorphine (0.1 mg/kg) and carprofen (5 mg/kg) dosages. The tissue was then carefully spread, and the cochleae were gently punctured using a borosilicate capillary pipette, which was kept in place to inject the following viral construct with its corresponding titer to the rats' cochleae: PHP.B_hSyn_Catch-EYFP at 9,49E+12 GC/ml (qPCR). After injection of the construct the tissue was repositioned, and the surgical lesion was then sutured. Carprofen (5 mg/kg) was administered for analgesia up until one day postsurgically.

Optically evoked auditory brainstem responses

For electrophysiological experiments, data sets were obtained from N = 10 adult wistar wild-type rats that received virus injections (see Postnatal AAV-injection into the rat cochlea) prior to optical stimulations and measurements in vivo. Surgeries and measurements were then performed 56.5 ± 2.27 days after injections. During surgeries animals were frequently monitored in regards of general isoflurane/air anaesthesia (3% for anesthesia induction, 0.6–2% for maintenance), the hind-limb withdrawal reflex, breathing as well as maintenance of physiological body temperature. Further, eye creme was applied and adjustments were made accordingly. Analgesia was provided by subcutaneous injections of buprenorphine (0.1 mg/kg body weight) every 4 hours and carprofen (5 mg/kg body weight). The injected cochleae were surgically exposed, performing a retroauricular incision and a bullostomy to ultimately puncture the round window's membrane of the animal in experiment. Then an optical fibre (200 µm diameter, 0.39 NA; Thorlabs) coupled to a 473 nm laser (MLLFN-473-100; Changchun New Industry Optoelectronics) was inserted via the round window for optical stimulations. Laser power was calibrated prior to each experiment using a laser power meter (Solo-2; Gentec-EO).

Stimuli were created, delivered and acquired using custom-written MATLAB (MathWorks, Inc.) script employing National Instrument data acquisition cards (NI PCI-6229; National Instruments) and a custom-built laser-controller. All measurements were conducted in a soundproof chamber (Industrial Acoustics). Optically evoked ABRs (oABRs) were measured by placing subdermal needle electrodes on the vertex (active electrode) and mastoid of the left (ipsilateral) ear (reference electrode), while active shielding (ground) electrode around tail region of the anesthetized rats. For all aABRs the difference in far-field potential between the subdermally inserted needle electrodes at the vertex and the left mastoid was amplified using a custom-designed amplifier. The sampling rate was at 50 kHz for 20 ms, and the signal was filtered (300–3000 Hz), and averaged across 1,000 stimulus presentations. The oABR thresholds were then defined as the minimum amount of light for the oABR amplitude to deflect and determined as the lowest light or sound intensity for which deflection was reliably visible.

The time between the stimulus onset and the peak of the wave of interest was defined as the latency. Further, amplitudes were determined as the difference in response strength between each corresponding positive (P) and the negative (N) peak.

The data characterising optogenetic stimulation of the rat cochlea (Supplementary figure 6) was processed and analysed using custom-coded MATLAB (The MathWorks, Inc.) scripts, Microsoft Office 365 (Microsoft Corp.), and GraphPad Prism 10.2.1. (GraphPad Software). Averages were expressed as mean ± SD, as specified.

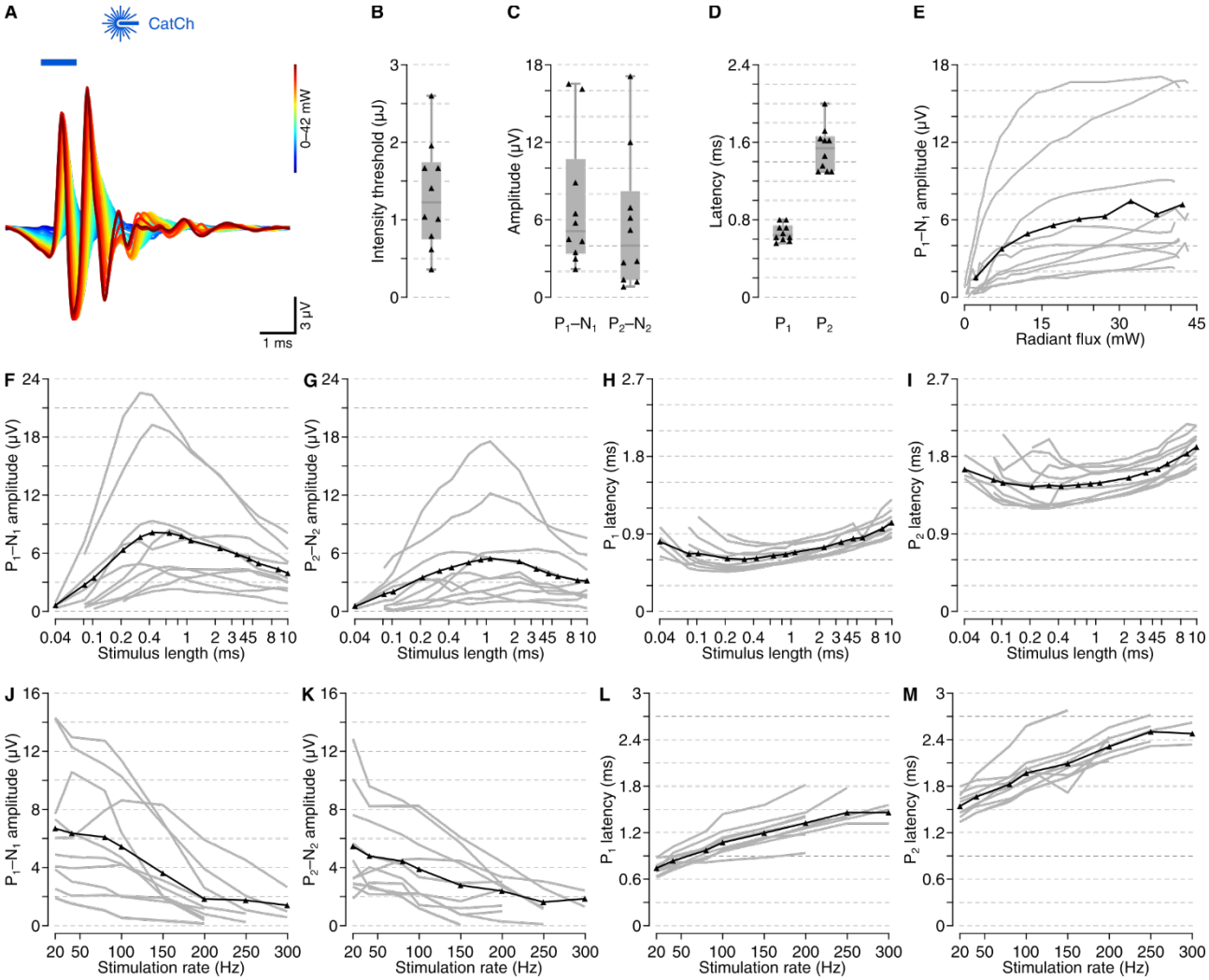

Supplementary figure 6. Characterisation of optogenetic stimulation of the rat cochlea expressing CatCh with auditory brain stem responses. (A) Exemplary optically evoked auditory brainstem responses (oABRs) elicited by pulses of various radiant flux (473 nm blue-light emitting laser, 1 ms pulses at 20 Hz, colour codes the radiant flux in mW) of injected rats with SGNs expressing CatCh-EYFP. Laser-coupled fibre was inserted via the round window. Blue bar indicates 1-ms-long stimulus (B to D) Analysis of characteristic parameters of CatCh-mediated oABRs with 1 ms 20 Hz pulses at 473 nm light for CatCh-injected rats (N = 10): intensity (radiant energy) threshold (B), P_1–N_1 vs P_2–N_2 amplitude (C), and P_1 vs P_2 latency (D). Data is presented as mean ± SD. Centre lines (dark grey) represent median values. Boxes (light grey) show the 25th and 75th percentile. Blue-light-activated CatCh (473 nm) was measured, using a maximum laser-output calibrated in a range of 38.8 to 43.6 mW (C and D). (E) P1–N1 amplitude as a function of radiant flux for all oABR measurements at 1 ms 473 nm light pulses of 20 Hz (grey lines), binned for mean values in 5 mW intervals (black line and markers). (F to I) Analysis of characteristic parameters of CatCh-mediated oABRs for various stimulus lengths using pulses at 20 Hz in a range of 38.8 to 43.6 mW (black: mean; grey: all measurements) for N = 10 rats: P_1–N_1 amplitude (F), P_2–N_2 amplitude (G), P_1 latency (H) and P_2 latency (I). (J to M) Analysis of characteristic parameters of CatCh-mediated oABRs at various repetition rates using 1 ms pulses at ~38 to 45.6 mW (black: mean; grey: all measurements) for N = 10 rats: P_1–N_1 amplitude (J), P_2–N_2 amplitude (K), P_1 latency (L), and P_2 latency (M).

Response rates in ShuttleBox detection task trails

We performed statistical analysis of response rates to a target and non-target trials in ShuttleBox detection task experiments (Supplementary figure 7; data as in Figure 3).

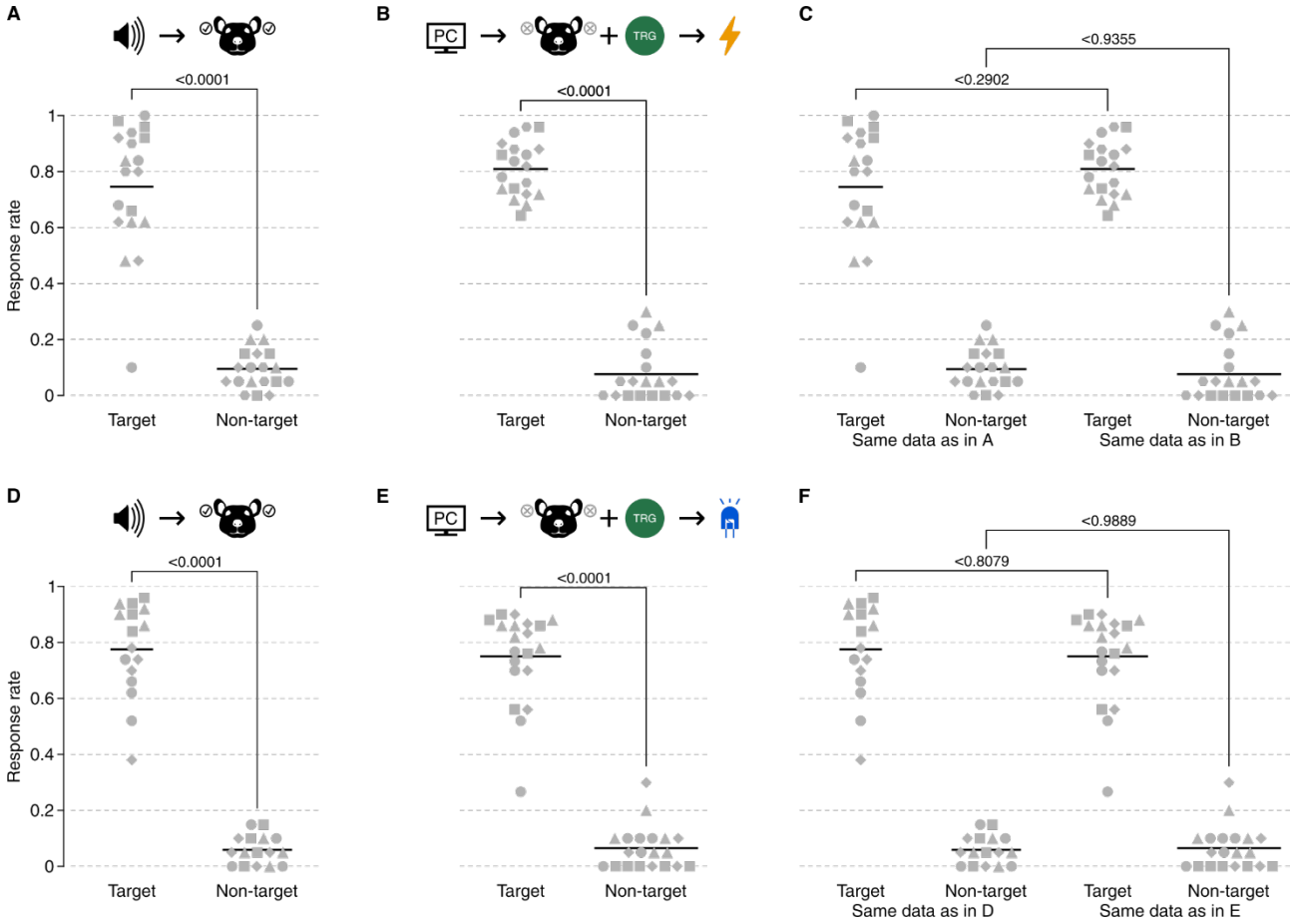

Supplementary figure 7. Analysis of behavioural responses to sound before and electrical (eCI) or optical (oCI) stimulation after deafening and implantation in target and non-target trial in the ShuttleBox detection task. (A to C) Comparison of target and non-target response rates to sound before and eCI stimulation after deafening and implantation. Response rate to target trials was significantly higher than to non-target trials in both acoustic (A) and electrical stimulation (B) sessions. Performance did not change after implantation (C). (D to F) Comparison of target and non-target response rates to sound before and oCI stimulation after deafening and implantation. Response rate to target trials was significantly higher than to non-target trials in both acoustic (D) and optical stimulation (E) sessions. Performance did not change after implantation (F). Data as in Figure 3. One-way ANOVA with Šídák's post-hoc test.

Auditory cued behaviour driven by an oCI system in partially deafened rat

We tested if real-time sound coding by oCI system can restore hearing in partially deafened (Supplementary figure 8) rats where some residual hearing was unintentionally maintained for lower frequencies (i.e. frequencies <16 kHz, high-frequency hearing loss). Hearing was evaluated before and after deafening by recording acoustic auditory brain stem responses (aABRs; Supplementary figure 8 A and B) as well as by the ShuttleBox paradigm (Supplementary figure 8 C). Using all LEDs inside the cochlea we aimed to restore hearing optically using both, *n*-of-*m* and CIS coding strategies, implemented into the NSV1 embedded software framework for $m = 8$ (Figure 5) or $m = 6$ (Supplementary figure 8) and $n = 3$ (in case of *n*-of-*m*; for details see main text, section “2.3. Sound coding strategy”). We set threshold level (TL) based on values estimated before (Figure 4). The most comfortable level (MCL) and a microphone gain were set based on the observation that operating all LEDs at intensity levels between 30–100 % triggered behavioural responses but no aversive behaviour like freezing or intensive scratching in the animals. We evaluated narrowband noise bands recruiting fewer LEDs (corresponding to frequencies ≥16 kHz) again, could demonstrate an auditory percept using oCI sound coding. In this animal, which could be considered as high-frequency hearing loss model, the sound-driven oCI-system elicited comparable response rates for impaired (8 kHz) and non-impaired frequency ranges (≥16 kHz; Supplementary figure 8 D and E). The operation of the oCI system was strictly required for the behavioural response: sound did not elicit the behaviour when the oCI was switched of (Figure 5 C and D, black line; Supplementary figure 8 C).

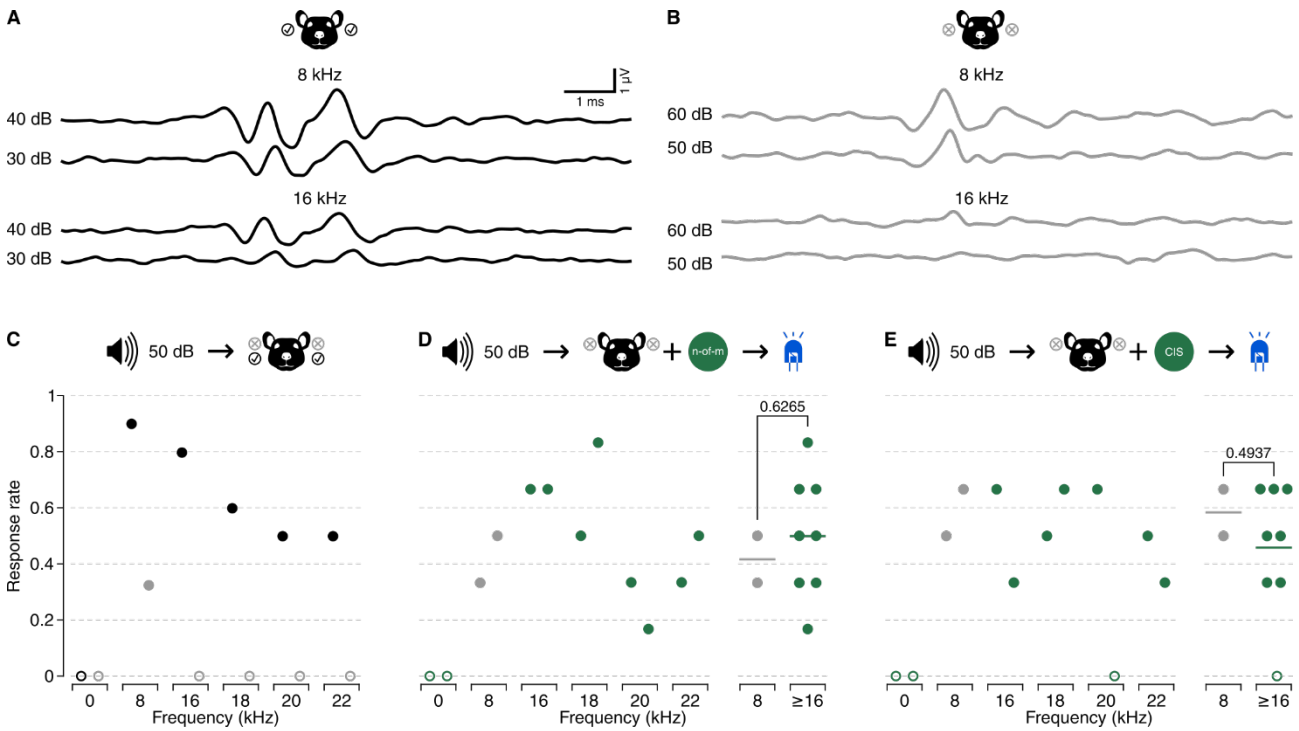

Supplementary figure 8. Auditory cued behaviour in a partially deafened rat driven by an oCI system using different coding strategies of the sound processor. (A and B) Representative acoustically evoked auditory brainstem responses (aABRs), in response to 8 and 16 kHz pure tones prior (A) and after (B) the implant surgery and deafening (black vs grey lines). All traces were recorded from the same animal. (C) Response rate to the acoustic stimulus in the ShuttleBox session of a trained hearing rat (black circles) and the same rat after deafening and oCI surgery without the sound processor (grey circles). (D and E) Results of two ShuttleBox sessions with activated sound processor encoding acoustic stimulus into light stimulus, either using *n*-of-*m* (*n* = 3 and *m* = 6 ; D) or CIS (*n* = *m* = 6; E) coding strategy in animal after deafening and oCI surgery (green circles; for frequencies ≥16 kHz, for lower frequencies some hearing was unintentionally maintained). The processing range of the sound coding strategy was adapted to the non-audible frequency range of the implanted rat (≥16 kHz) and the processor encoded those using 8 LEDs inside the cochlea of the AAV-transduced rat. Filled circles correspond to response rate of one complete ShuttleBox session whereas empty circles emphasize the lack of any response on the behavioural level. While for implanted rat behavioural response was always observed for 8 kHz (D and E, grey circles), a frequency also showing a response in the aABR after surgery (B), behaviour in response to pure tones at 16, 18, 20, and 22 kHz was only observed when the processor was turned on. The sound-driven oCI-system elicited comparable response rates for impaired (8 kHz) and non-impaired frequency ranges (≥16 kHz; D and E right panels; unpaired, two-tailed t-test). All acoustic stimuli were presented at 50 dB.

References

[1] Arm Software CMSIS Version 5

[2] Gossler C, Bierbrauer C, Moser R, Kunzer M, Holc K, Pletschen W, Köhler K, Wagner J, Schwaerzle M, Ruther P, Paul O, Neef J, Keppeler D, Hoch G, Moser T and Schwarz U T 2014 GaN-based micro-LED arrays on flexible substrates for optical cochlear implants *Journal of Physics D: Applied Physics* **47** 205401 DOI: 10.1088/0022-3727/47/20/205401

[3] Wiegner A, Wright C G and Vollmer M 2016 Multichannel cochlear implant for selective neuronal activation and chronic use in the free-moving Mongolian gerbil *J. Neurosci. Methods* **273** 40–54 DOI: 10.1016/j.jneumeth.2016.08.006

[4] Schwaerzle M, Nehlich J, Ayub S, Paul O and Ruther P 2016 LED-based optical cochlear implant on highly flexible triple layer polyimide substrates *2016 IEEE 29th International Conference on Micro Electro Mechanical Systems (MEMS)* 2016 IEEE 29th International Conference on Micro Electro Mechanical Systems (MEMS) (Shanghai, China: IEEE) pp 395–8 DOI: 10.1109/memsys.2016.7421644

[5] Keppeler D, Schwaerzle M, Harczos T, Jablonski L, Dieter A, Wolf B, Ayub S, Vogl C, Wrobel C, Hoch G, Abdellatif K, Jeschke M, Rankovic V, Paul O, Ruther P and Moser T 2020 Multichannel optogenetic stimulation of the auditory pathway using microfabricated LED cochlear implants in rodents *Sci Transl Med* **12** eabb8086 DOI: 10.1126/scitranslmed.abb8086

[6] Huet A T and Rankovic V 2021 Application of Targeting-Optimized Chronos for Stimulation of the Auditory Pathway *Methods in Molecular Biology (Clifton, N.J.)* vol 2191 pp 261–85 DOI: 10.1007/978-1-0716-0830-2_16

[7] Kleinlogel S, Feldbauer K, Dempski R E, Fotis H, Wood P G, Bamann C and Bamberg E 2011 Ultra light-sensitive and fast neuronal activation with the Ca2+-permeable channelrhodopsin CatCh *Nat Neurosci* **14** 513–8 DOI: 10.1038/nn.2776